# International Conference on Space Optics—ICSO 2022

Dubrovnik, Croatia

3–7 October 2022

*Edited by Kyriaki Minoglou, Nikos Karafolas, and Bruno Cugny,*

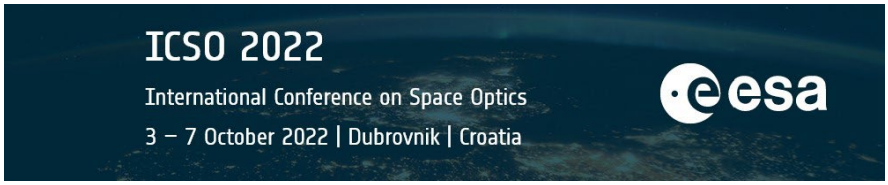


# *Towards space qualified Spatial Light Modulators for optical compact instrumentation*


International Conference on Space Optics — ICSO 2022, edited by Kyriaki Minoglou, Nikos Karafolas, Bruno Cugny, Proc. of SPIE Vol. 12777, 127775Z · © 2023 ESA and CNES · 0277-786X · doi: 10.1117/12.2691106

# Towards space qualified Spatial Light Modulators for optical compact instrumentation

Manuel Silva-López*, Alberto Álvarez Herrero
Instituto Nacional de Técnica Aeroespacial (INTA), Dpto. de Óptica Espacial, carretera de Ajalvir, Km 4, Torrejón de Ardóz, 28850 Madrid, Spain

## ABSTRACT

Spatial Light Modulators (SLM) are electro-optical devices based on liquid crystal (LC) properties. One of the most common type is the reflective LC on a ship display, where the LC molecules are sandwiched between a silicon pixel, and a transparent electrode. Upon illumination, the phase of the light reflected is modulated according to the molecular alignment, which is controlled, pixel by pixel, using a CMOS backplane.

These devices have a high potential for space applications due to the fact that they allow to introduce any tailored wavefront distortion in an imaging instrument. Indeed, image reconstruction methods as phase diversity, for example, can be used to determine inflight the Point Spread Function and, later, introduce a corrective wavefront distortion to correct deviations of the expected optical quality. On top of that, adaptive optical systems, focusing correction, beam steering or communication systems based on modulating phase/polarization can be easily implemented using this technology.

Moreover, the compactness and low power requirements of SLMs can be of great advantage for small satellites with onboard optical instrumentation. SLMs can save complexity and weight and it also reduces the risk associated to the wear of moving parts. However this technology has not been qualified for space applications. Our group has a solid background on the development of liquid crystal devices for space applications (i.e.: the polarization modulators onboard two instruments of the Solar Orbiter mission). Thus we aim to use our knowledge to obtain a full space qualified SLM.

In this work we have explored the robustness of different SLM models under environmental tests of particular interest in space applications. The tests concerned with this work are a vibration test (sinusoidal and random), an operative thermo-vacuum test with a range of temperature from 30°C to 60°C; and a gamma irradiation test with accumulative doses up to 100 krad(Si). Several indicators, such as the retardance versus voltage curve, the optical flatness and time response, are monitored before and after each environmental test. Out-gassing and a non-operative thermal test have been also investigated. The SLMs successfully passed all the tests and no degradation was observed. These space simulation tests show that SLM is a valid and robust technology with a large potential to perform a great number of optical space applications. This is also a previous step towards a specifically application designed and space qualified SLM.

**Keywords:** Spatial light modulator, liquid crystal, phase shifting, space environment, vibration test, vacuum compatibility, COTS

## 1. INTRODUCTION

A liquid crystal on silicon (LCoS) is an electrically addressed, reflection type, phase 2D spatial light modulator (SLM). SLMs yield a structure where a liquid crystal layer, serving as the light modulating part, is arranged on an electrically addressing part formed by CMOS technology, i.e. liquid crystal is controlled by a direct voltage, and can modulate the wavefront of a light beam. They have found applications in optical beam shaping, aberration correction, optical metrology and laser material processing [1].

In space applications, where resources such as mass, volume, power consumption and reliability are fundamental issues; there is a strong demand on photonic devices. Moreover, liquid crystal variable retarders (LCVR) based devices, in particular, can save complexity and weight, they may be implemented to avoid mechanical parts on spacecraft optical instrumentation. Indeed some preliminary tests were published evaluating the space survivability of this technology [2]. Nevertheless, and following this aim, in our group we performed an extensive validation and qualification campaigns of polarization modulators based on LCVRs for aerospace applications and, currently, they are being operated onboard the

*silvalm@inta.es

Solar Orbiter ESA mission [3-6]. As a consequence, LCVRs developed by us reached a Technology Readiness Level (TRL) 9, "Actual system proven in operational environment" [7]. To achieve this, however, different liquid crystal cells were first analyzed under specific environmental conditions. Thus the technology is checked against the expected mission environment, reaching TRL5 "Component Validation in Relevant Environment". In a second step, and after being included in the baseline design of the Solar Orbiter instruments, qualification and acceptance campaigns of the polarization modulators were carried out to be finally approved for flight [8, 9].

Building on the legacy of the polarization modulators developed, the natural step forward is to extend this approach, exploiting our background on liquid crystal devices, to validate SLM technology. Among other applications, SLMs allow the development of non-mechanical laser beam steering technology, suitable for stablishing satellite-to-ground data links [10], they may also produce orbital angular momentum modulation for deep-space optical communications [11]. Recently, adaptive hyperspectral imaging using SLMs for space applications has been proposed [12].

However this technology remains to be validated for space applications. Our previous work have shown potential compatibility [13]. However, in this work we focus on commercial-off-the-shelf (COTS) SLMs display modules, leaving aside the control and conditioning electronics not relevant for our purpose. In the rest of this section we define the performance indicators that will allow to monitor the performance of the devices under test. Section 2 describes these devices: They are two different SLM models with a very compact display that is connected to the driver by a flexible cable. Preliminary measurements are shown from both models and the validation plan is outlined. We set these devices to the main tests required for space application validations: Section 3, 4 and 5 deal with the thermal vacuum, vibration and gamma irradiation tests respectively. Section 6 describes other preliminary tests performed on another SLM unit. Finally a discussion on the results follows.

### 1.1 Performance indicators

To begin with a number of *performance indicators* shall be defined. They set the 'state of health' of the device, these are retardance versus voltage calibration curve, the retardance spatial homogeneity (flatness) and the response time. Among different measuring techniques [14] we have chosen to use a phase shifting interferometric technique to evaluate the first performance indicator. It is relevant to note that, for the retardance versus voltage curve, a two segments approach was used, as described in [15].

A liquid crystal cavity may change with external pressure and temperature. Moreover, due to fabrication limitations, the CMOS back plane and glass substrate of the SLM may not be flat nor parallel. Thus, an inspection of the surface flatness of the SLM is mandatory during the tests, and this was performed by fringe pattern analysis. Finally, the response time was evaluated using a polarimetric method, as we will explain later.

## 2. SLM DESCRIPTION & VALIDATION PLAN

In our work we have used two SLM models from HOLOEYE Photonics AG: these are the HED6010-VIS-016-C and HED6010-VIS-096-D. Both displays have an active area of 15.36 mm × 8.64 mm, with 1920 × 1080 pixel resolution. They have an 8 μm pixel pitch with 256 gray levels (8 bit), and both models have a wavelength range of 450-650 nm. They are connected via a flexible bus cable, and can be controlled by a HOLOEYE driver (PLUTO-2 model). The driver processes the images generated at the PC, (HDMI connection) and sends the suitable control signals to the SLM display. The frame rate is 60 Hz and the drive scheme is pulse code modulation.

However the displays are different in terms of LC material, cell thickness, alignment layer (VIS-016 is polymide and VIS-096 is $SiO_x$) and LC mode (VIS-016 is PAN and VIS-096 is VAN). The packaging is also different: The VIS-016 LCoS cell is attached to a PCB (with plated-through holes) that is attached to a metal base plate. On the contrary, model VIS-096 has the LCoS cell attached to a ceramic substrate. Both displays have a flexible cable that is attached to the driver by a ZIF connector.

As a consequence of their fabrication differences, each display requires a specific calibration file to obtain a linear phase-voltage relation (set from 0 to 2.1π). This is achieved with a calibration curve with voltage range of [0.89V - 1.52V] and [2.60V - 4.85V] for the VIS-016 and VIS-096 display models respectively. This calibration is always performed before using each SLM model.

Prior the test we have measured flatness and retardance at laboratory conditions. Results for each model are presented in Table 1. Also retardance was evaluated from 30 to 60ºC: both models have a remarkable thermal stability and they show no changes in retardance with temperature within their operational thermal range.

Table 1. Prior measurements before environmental tests.

| SLM model | Retardance versus voltage | Rad/ grey level | Flatness measurement | Waves (λ) |
|---|---|---|---|---|
| VIS-096 | Slope | 0.0250 | PV | 3.57 |
| | RMSE | 0.116 | RMS | 0.49 |
| VIS-016 | Slope | 0.0247 | PV | 5.16 |
| | RMSE | 0.141 | RMS | 0.94 |

For the purpose of technology validation the process requires indeed the procurement of a number of identical devices, and they are to be inspected or tested in accordance with space standards [16]. We have, however, a limited number of different units available. Nevertheless, the differences in the displays are interesting in terms that it shows that this technology is robust within a range of specifications. As a consequence, and according to the positive results obtained during these tests, we consider these exploratory tests very relevant.

Thus, the displays have followed the tests in the order described in Table 2. It is important to remark that the tests were performed on the displays, not the driver. In this sense, the ease of connection/disconnection process and the displays compactness are very handy. With each environmental test follows, in turn, a different procedure, as shall be explained. In general, however, the procedure involves measurement of the performance indicators before and after each test. However for the thermal vacuum test, they are also evaluated during the test.

Table 2. Environmental tests for each model

| SLM model | 1st environmental test | 2nd environmental test |
|---|---|---|
| VIS-096 | Operative thermal vacuum | Gamma irradiation |
| VIS-016 | Vibration | |

# 3. THERMAL VACUUM TEST

## 3.1 Test set up description

As mentioned, the SLM model VIS-096 was subjected to thermal-vacuum conditions and the three performance indicators were obtained at different temperatures. The test conditions are a pressure of $10^{-5}$ mbar at the target temperatures of 30ºC, 40ºC, 50ºC and 60ºC. To thermalize the device the SLM was attached to a metal block. Figure 1 a) shows a view of the SLM display within the thermo-vacuum chamber. A PT100 thermal sensor and a heater were also fixed to this same block (at the backside). Thus, a thermal control system (PID) uses these thermo-electric elements to keep the system at the temperature set point. Nevertheless, the SLM temperature can be read by an internal thermistor embedded. During the test, however, it was found an increasing discrepancy among the thermistor and the PT100 readings. A conservative approach was chosen in which none of the sensors reached the maximum operative temperature specified by the manufacturer (70ºC).

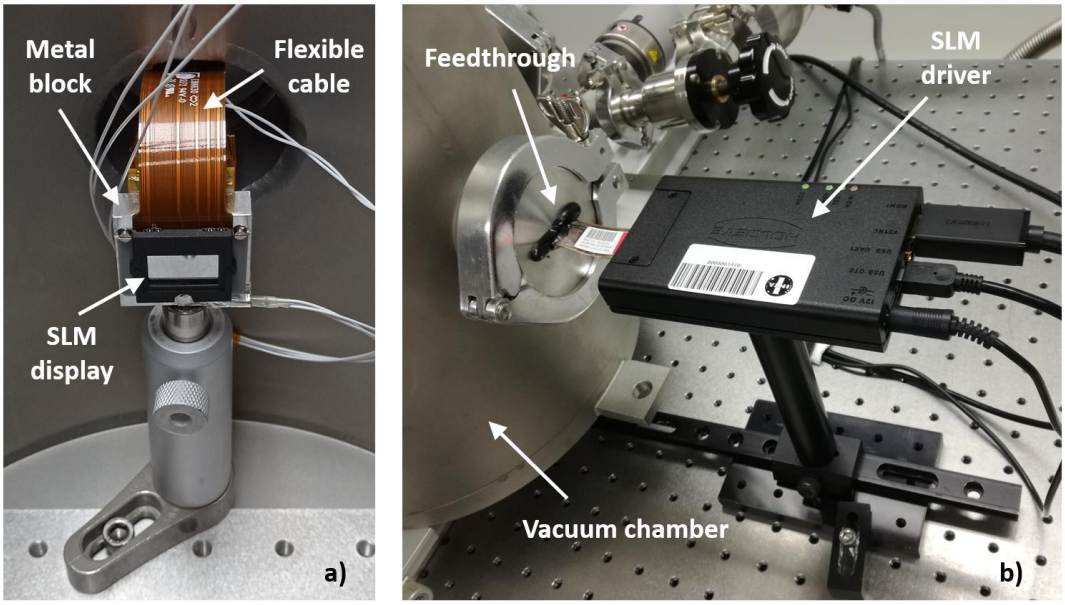


Figure 1. a) SLM display within the vacuum chamber. b) View of the SLM driver at the outside of the chamber, and a view of the dedicated feedthrough.

To simulate the space environment a thermal vacuum chamber was used. The chamber has a cylinder shape with 26 cm of inner diameter and 28 cm height. A primary pump and a turbo-molecular pump (Varian, Turbo-V 81-M) set the vacuum levels required for the tests. The chamber also provides feedthroughs for connections to thermo-electric elements. It has an optical window that allows the laser beam to reach the SLM display. Figure 1 b) shows a view of the outside of the chamber, where a dedicated feedthrough, built to interface the SLM display with the driver can be seen.

A diagram of the optical experimental setup is shown in Figure 2. A He-Ne laser beam is expanded and collimated to cover the SLM effective area. A beam splitter folds the SLM reflected light path so that a camera (Pantera TF 1M30 model from DALSA) is illuminated. A reference mirror, also shown in Figure 2, is used to set up a Michelson interferometer arrangement. SLM driver and camera were connected to a computer, and controlled using MATLAB. The PT100 sensor reading was used by the PID system to set the target temperature. Finally, an SLM embedded thermistor, which can be read by the HOLOEYE software, was also monitored.

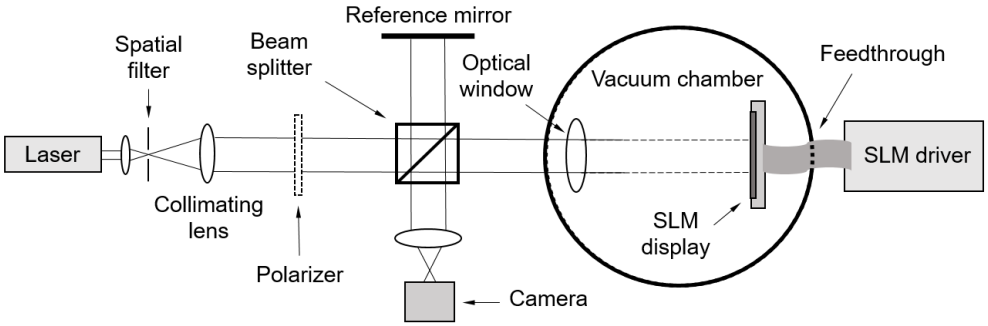


Figure 2. Set up configuration employed to obtain the phase modulation characteristic and surface flatness measurements. This setup is then adapted to perform response time measurements.

### 3.2 Optical results of thermal vacuum test

Figure 3 shows the retardance versus voltage measurements obtained at the temperature setpoints. For this performance indicator we have used a modified phase shifting technique, as described in [15]. It is interesting to note that, as temperature was increase, a larger discrepancy was found between both thermal sensors. This may be due to thermal gradients, and PT100 sensor lower thermal contact. Thus in the plot we provide both readings. Temperatures shown in Figure 3 correspond to the set point commanded to the PID system and, within brackets, the embedded thermistor reading. The measurements do not show a significant temperature sensitivity. This is remarkable since no temperature compensation is performed by the system.

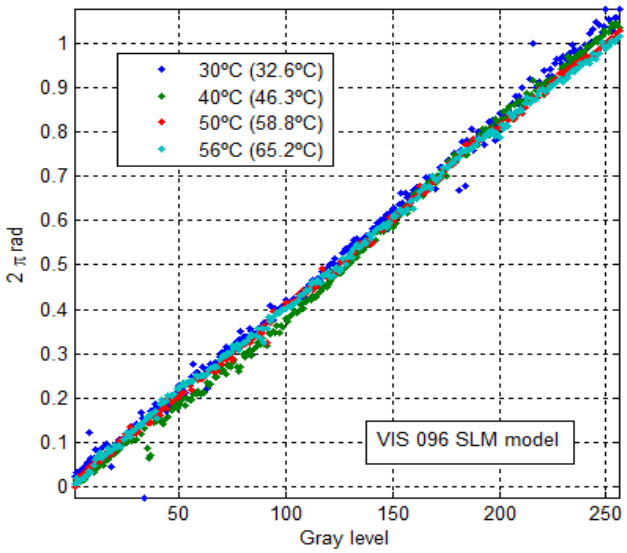


Figure 3. Retardance versus voltage curves of the VIS-096 at different temperatures and $10^{-5}$ mbar pressure.

To measure the time response of the SLM we have used a modified version of the set up shown in Figure 2. We blocked the reference mirror optical path and add a polarizer, at the incident beam, at 45º with respect to the SLM optical axis. Reflected light goes through an analyzer and hits a photodetector. An oscilloscope (1 GHz 5GSa/s) captures light intensity as 2π phase transitions are commanded. After processing the light intensity output measurements, we obtain the activation and relaxation time of the SLM at each temperature. In Figure 4 we can see the phase response at 30ºC as an example. In Table 3 we summarized the response time measured at each temperature. The response time is clearly smaller as the temperature increases following a decreasing exponential behavior as expected.

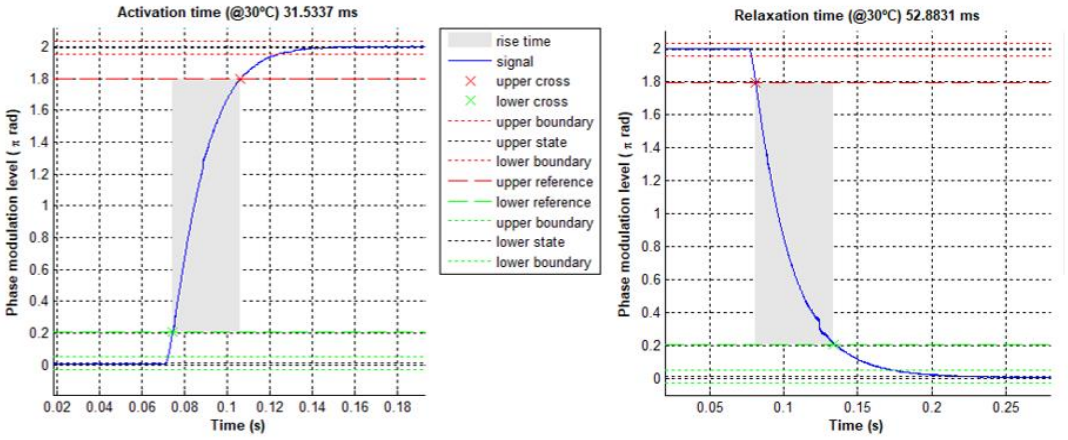


Figure 4. Rise and fall time as measured from a 2π phase jump/transition at vacuum conditions and 30ºC

Table 3. Summary of transient times at each temperature

| Temperature (ºC) | 30 ºC | 40 ºC | 50 ºC | 60 ºC |
|---|---|---|---|---|
| Activation time (ms) | 31.53 | 20.79 | 15.93 | 12.87 |
| Relaxation time (ms) | 52.88 | 33.35 | 26.37 | 22.64 |

Finally, measurements of the SLM surface flatness were performed during this test. Figure 5 shows the wavefront reconstruction at the temperature setpoints. To highlight changes we have subtract the wavefronts from the coldest and hottest case.

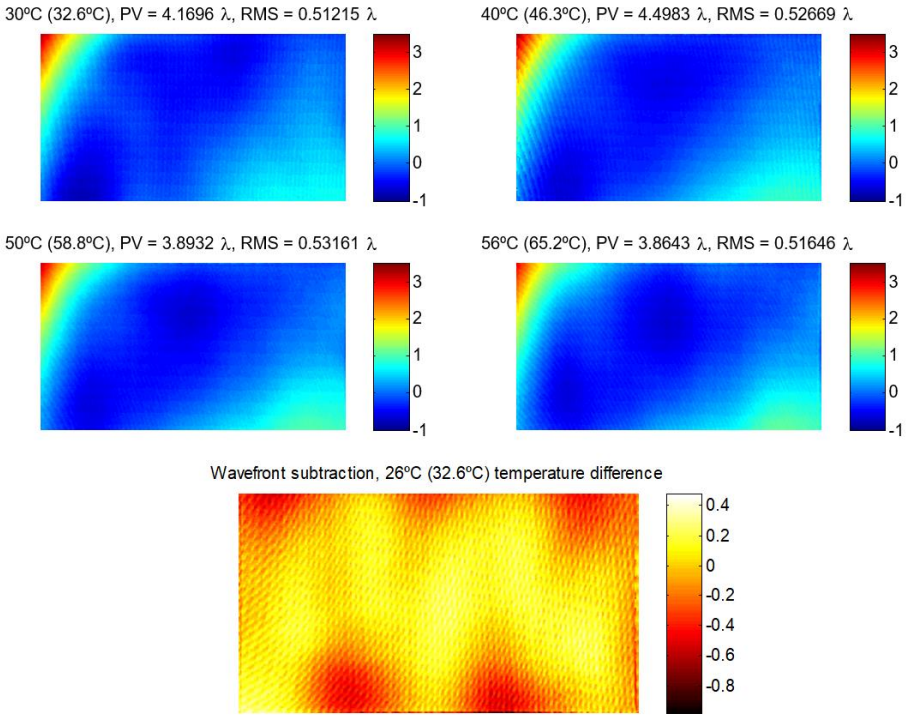


Figure 5. Upper panels) Display flatness evaluated at the temperature set-points and $10^{-5}$ mbar pressure (in waves). Lower panel) Subtraction of the flatness evaluated at ~30ºC and ~60ºC temperature. This is a 26ºC (32ºC) temperature difference according to the PT100 (thermistor) sensor.

# 4. VIBRATION TEST

A vibration test is mandatory in every space equipment test sequence [17]. This is typically a sinus vibration test (often an acceleration test, if not included in the sinusoidal test) and a random and/or acoustic vibration test. In our test we have used the VIS-016 model, and performed sine and random vibration tests on three SLM orthogonal axes.

The test levels chosen for this device are similar than those used during the LCVR calification process for the Solar Orbiter mission [18]. However, for the sine vibration levels, we have expanded the band to accommodate the requirements for qualification at equipment level described in [17]. The final values are presented in Table 4. It is important to note that these levels are independent of the axis, i.e., no in-plane or out of plane position is assumed.

Table 4. Sine and random vibration test levels

| | Band | Level |
|---|---|---|
| Sine vibration test levels ( 2 Oct/min per axis) | 5 – 20 Hz | 11 mm |
| | 20 – 140 Hz | 25 g |
| Random vibration test levels (120 s per axis) | 20 – 100 Hz | +3 dB/Octave |
| | 100 – 400 Hz | 0.6 $g^2$/Hz |
| | 400 – 2000 Hz | -6 dB/Octave |

The allowable tolerances for sinusoidal and random vibration levels are taken from [17]. Moreover, in order to evaluate the equipment integrity, and according to this standard, a resonance search is performed before and after each random and sinusoidal vibration test.

Thus, the tolerances for sinusoidal test in the 5 Hz to 2000 Hz frequency range is ± 2 % (or ±1 Hz whichever is greater). The amplitude and sweep rate (Oct/min) is ± 10 % and ± 5 % respectively. On the other hand, the random vibration allowable tolerances for amplitude are < ± 3 dB, for the whole frequency range, and the random overall $g_{rms}$ is ± 10 %.

### 4.1 Vibration test description

Thus, in this test we perform sinusoidal and random vibrations along different SLM axes. However, to begin with, the display is connected to the driver at the optics laboratory. Flatness and optical retardance are evaluated using the interferometric arrangement described in Section 3 (at normal conditions). Figure 6 a) shows the SLM unit ready for optical measurements. Then the SLM is taken to the vibration facility and fixed at a certain orientation. After vibration the SLM is placed back within the interferometer and optical measurements are performed again. This process is repeated.

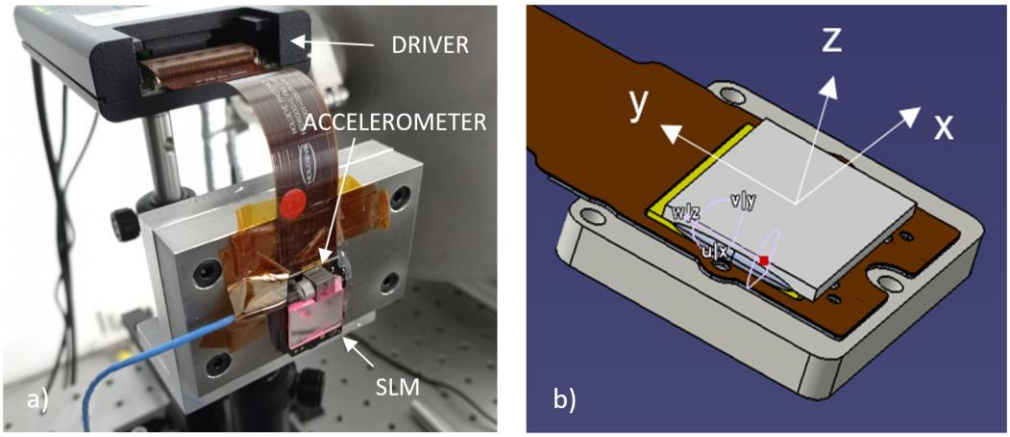


Figure 6. a) SLM plugged to the driver and ready for optical measurements. The display has been glued to a metal block that eases the test. A triaxial accelerometer has been also glued next to the active area of the SLM. b) SLM reference axes.

As mentioned the procedure includes the vibration test along three orthogonal axes of the SLM. These axes are defined in Figure 6 b) where a CAD image of the SLM is shown with the reference axes. The SLM display is in the *x*-*y* plane, and the *z*-axis is orthogonal. We have performed the same vibration procedure on each axes. This is the first time to our knowledge that this procedure has been followed by an SLM.

Figure 6 a) also shows that the SLM is glued to a small plate (10×50×80 $mm^3$ aluminum block). This is relevant since it allows to be attached at different positions at the vibration tool, as we shall see. Also a triaxial accelerometer was glued next to the active area of the SLM. This sensor will be used to monitor the actual vibrations followed by the unit.

The tests were performed with a one-axis vibration stage. On top of it a cube shaped vibration tool is attached. This tool allows to fix the SLM at different orientations. Thus achieving the 3-axis SLM vibration, one at a time. Figure 7 shows the three configurations on top of the vibration stage.

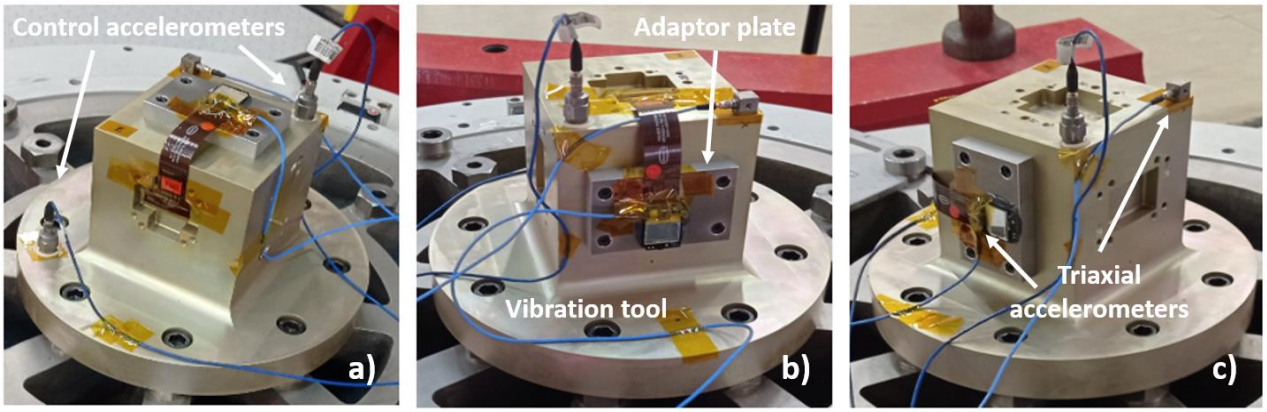


Figure 7. SLM attached to the vibration tool in different configurations. SLM main vibration is performed in the a) *z* axis, b) *y* axis and c) *x* axis

Two ‘control’ accelerometers are attached to the vibration tool according to Figure 7. A triaxial accelerometer is also attached to the vibration tool, this sets the reference axis of the vibration tool (vibration in the z-axis). The triaxial accelerometers are from PCB Piezotronics, (model 356A01 SN LW165935 the SLM one). Finally. the SLM alone has a weight of 7.6 g. However, the set formed by the SLM, plus the adaptor plate, the accelerometer and glue has a weight of 152 g. Alternatively, the vibration tool has a weight of 7550 g, fifty times more. Thus we do not expect any interference.

### 4.2 Vibration charts

By means of the triaxial accelerometers we obtain data for each vibration axis, in any of the three arrangements described. Typical vibration charts are shown in Figure 8. Here we plot the SLM triaxial accelerometer data obtained during the test. This data corresponds to the SLM *x*-axis parallel to the vibration axis, which is the arrangement shown in Figure 7c). Left and right plots of Figure 8 correspond to the sinusoidal and random test measurements respectively. Both plots show that the target levels were clearly followed within the allowable tolerances. The orthogonal *y* and *z*-axes show minor residual vibrations.

Data for SLM vibration in the *y* and *z*-axis are similar to the one presented in Figure 8. Overall the vibration tests were successfully performed and no damage was observed in the SLM after visual inspections. The next section shows the optical measurements performed after vibration of each axis.

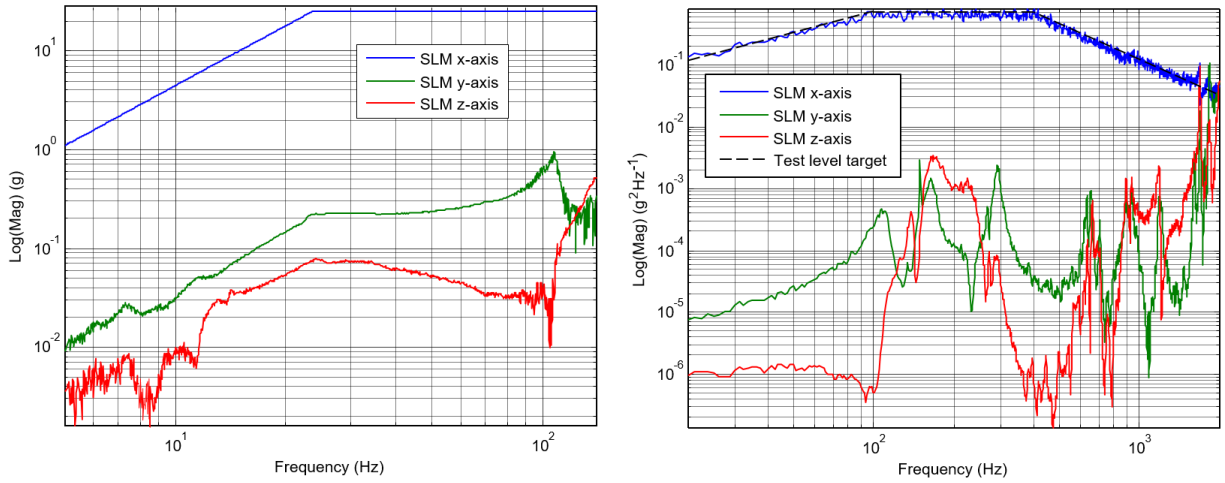


Figure 8. Vibration charts obtained from the triaxial accelerometer attached to the SLM. This data corresponds to the arrangement where the vibration axis was the *x*-axis. Left and right plot shows the sine and random test respectively in their given frequency ranges. The target vibration levels were clearly followed.

### 4.3 Optical results of the vibration tests

As mentioned, the retardance versus voltage curve and flatness are evaluated after vibration of each SLM axis. This implies removing the display from the vibration tool, setting the interferometer arrangement and connecting the display to the driver. This may affect measurement repeatability. Thus the retardance versus voltage curve at each stage during the vibration test is shown in Figure 9. Clearly the *y*-axis curve drops off a little. This slope difference may be due to some experimental errors. Nevertheless, and since the first and last measurement match well, we conclude the device has not degraded.

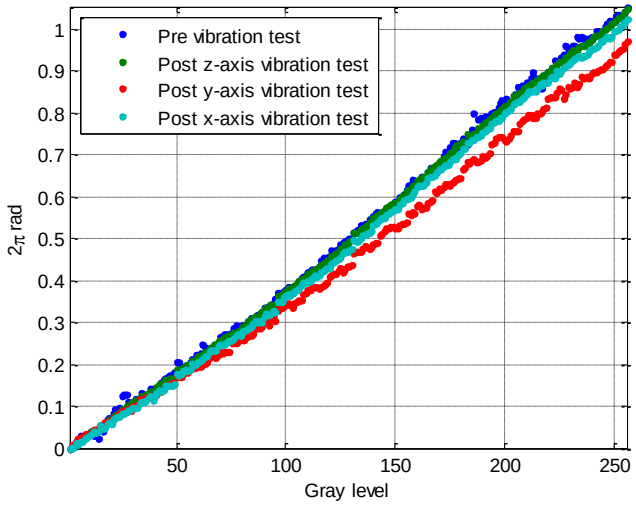


Figure 9. SLM calibration curve obtained at different stages during the vibration tests.

Figure 10 shows the flatness recovered by the experimental set up. The PV value is more sensitive to changes of the experimental conditions. This can be seen when we compare the values from the pre-test measurement and data from the Table 1. Setting up and optical realignment may be a non-negligible source of measurement uncertainty. In any case, and during the test, the RMS value showed low variations among measurements.

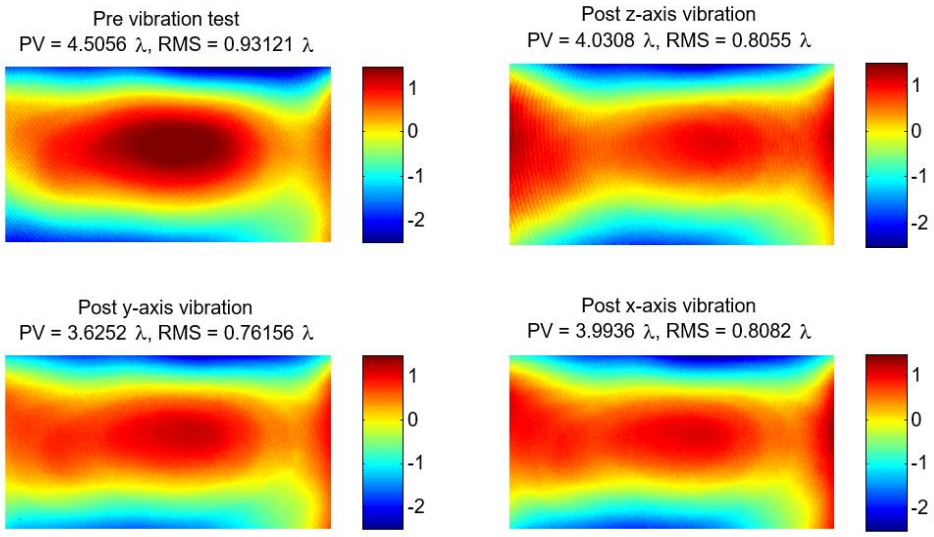


Figure 10. SLM VIS-014 flatness measurements in waves at different stages during the vibration tests

## 5. GAMMA IRRADIATION TEST

The SLMs ionizing irradiation tests were performed at the NAYADE Gamma Irradiation Facility, in Centro de Investigaciones Energéticas, Medioambientales y Tecnológicas (CIEMAT), in Madrid. Here, a $^{60}$Co sources are used inside a water pool at atmospheric pressure and room temperature. Samples can be encapsulated in a cylinder and deployed at the adequate distance to fulfill with the specified dose rate, as was calibrated in a dosimetry check (4.989 krad (Si)/h).

A portable interferometric setup was built to perform the intermediate optical control measurements (phase-voltage curve and optical flatness). The units undergone 5 intermediate doses of gamma radiation in order to assess the tolerance of the SLMs to ionizing radiation: 10, 25, 50, 75 y 100 krad (Si). These levels are taken from the values applied for our LCVR technology validation [8-9]

### 5.1 Test description

In this test both SLM models were employed. As shown in Figure 11 a), the SLMs were attached so that the displays are next to each other. The arrangement ensures that the accumulated doses received were homogeneous better than 90%. Thus, the sample holder was located inside the underwater casing. The figure shows the arrangement before it is inserted in a watertight cylinder, with both displays side by side. Then this is submerged and kept at the adequate distance as shown in Figure 11 b).

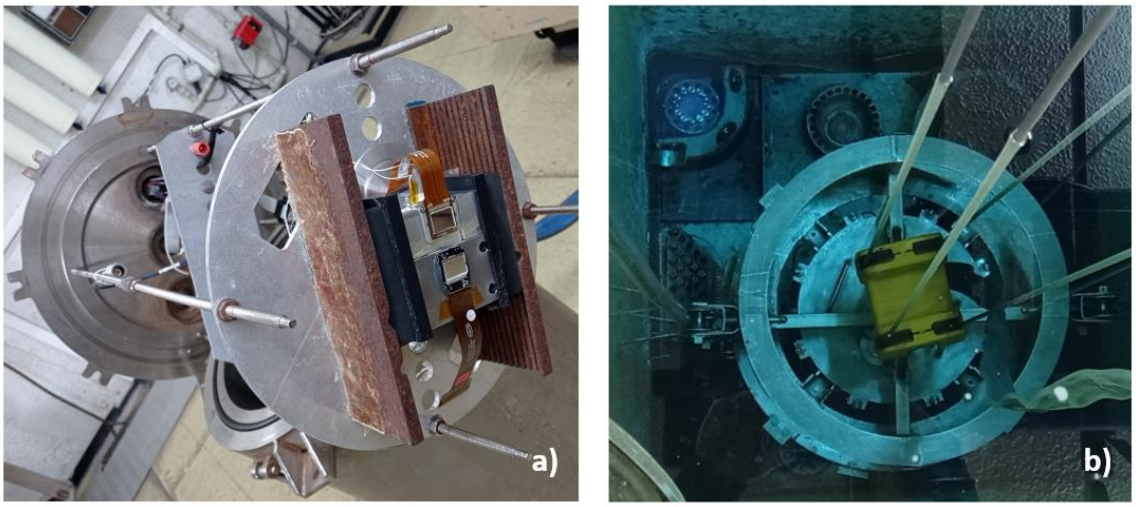


Figure 11. Gamma irradiation set up. a) The SLMs are arranged so that they can be encapsulated in a cylinder. b) Cylinder case deployed at the bottom of the bottom of the water pool, on top of gamma sources.

Once irradiation is performed, by suitable exposition time, the displays are recovered and inserted within the interferometer arrangement. Then the retardance versus voltage and flatness are evaluated for both models. The devices are also set to a fixed temperature (±0.5ºC) by means of a thermal control system. The arrangement allows access to the cables to be able to connect the SLM driver. This is important in order to perform optical checks during the irradiation stages. The process is then repeated but for a higher gamma irradiation doses.

### 5.2 Optical results of gamma irradiation

Figure 12 shows the retardance versus voltage measured after each irradiation test, and SLM model. These results are consistent with [2], which showed that gamma irradiation only produces a shift of the retardance versus voltage curve from 1000 Krad. On the other hand polymide layers were shown very good radiation hardness up to a total gamma dose of 10000 Krad. Finally flatness measurements, listed in Table 5, show very good stability. No degradation can be inferred from this data.

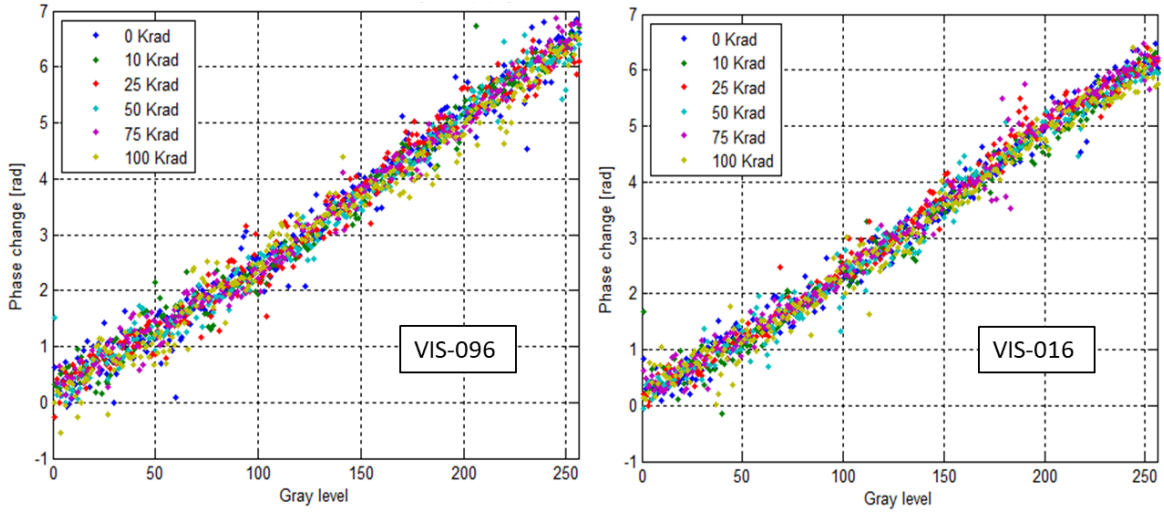


Figure 12. Phase voltage characteristic as a function of accumulated doses for each SLM model [5 krad (Si)/h]

Table 5. Summary of flatness measurement results

| | | Pretest | 0 Krad | 10 Krad | 25 Krad | 50 Krad | 75 Krad | 100 Krad |
|---|---|---|---|---|---|---|---|---|
| VIS-016 | PV **(λ)** | 5.16 | 5.07 | 5.21 | 4.65 | 4.97 | 5.16 | 5.00 |
| | RMS **(λ)** | 0.942 | 0.884 | 0.970 | 0.838 | 0.870 | 0.925 | 0.888 |
| VIS-096 | PV **(λ)** | 3.57 | 3.24 | 4.36 | 3.78 | 4.27 | 4.47 | 4.55 |
| | RMS **(λ)** | 0.497 | 0.556 | 0.755 | 0.680 | 0.814 | 0.745 | 0.712 |

## 6. OUTGASSING AND NON-OPERATIONAL THERMAL VACUUM TEST

We have also performed preliminary tests on other aspects relevant to SLM space compatibility. For instance, another HOLOEYE SLM non –functional model, the VIS-014, was set to vacuum conditions ($10^{-6}$ mbar) during four hours with molecular organic contaminant monitoring. Less than 10 ng $cm^{-2}$ of hydrocarbon and methyl-silicone were measured. With ester or phenyl-meth-silicone outgassing negligible. The same model was later subject to a non-operative thermal-vacuum test. The unit was set to -15ºC and 70 ºC. Afterwards visual inspection showed no damaged. Since this was a non-functional device we could not perform electro-optical tests, however, to check outgassing, LC leaks or cracks this is a valid model.

## 7. CONCLUSIONS

In the present work, a number of environmental tests, of utmost interest for space applications, have been performed on two commercial SLM models. They were an operational test under thermal-vacuum conditions, an equipment-level vibration test and a gamma irradiation test. As far as we know, this is the first work on the survivability of SLMs under this set of space simulation tests. The analysis on their influence were performed by measuring the optical retardance, the display flatness and the response time.

At room conditions both models are very insensitive to thermal variations within the operating range: However, the model VIS-096 show excellent performance at thermal-vacuum conditions ($10^{-5}$ mbar at 30 to 60ºC). VIS-016 model also show good repeatability after vibration for qualification at equipment level in three orthogonal axes. Finally, both models have been gamma irradiated and no degradation was also appreciated with accumulative doses up to 100 krad (Si). Overall, it has to be noted that the devices under test have performed well, and that no degradation can be inferred from the experimental measurements. In general, it can be concluded that, from the results obtained, SLM are compatible and suitable for space instrumentation. This is remarkable since these are COTS devices, not optimized whatsoever.

Further work remains to fully qualify a specific model. However, these space simulation tests show that SLM is a valid and robust technology with a large potential to perform a great number of optical space applications. Indeed, and according to the milestones demonstrated in these tests, we may conclude that critical functions of the SLMs have been demonstrated in a relevant environment. This is a basic requirement for enabling a TRL5. This is also a previous step towards a specifically application designed and space qualified SLM.

## ACKNOLEDGEMENTS

The authors would like to express their gratitude to HOLOEYE Photonics AG for their support and for kindly providing SLM models for tests. We also acknowledge the Spanish Solar Physics Consortium (S3PC, Red Española de Física Solar Aeroespacial) and, in particular Antonio Campos-Jara, the Vibration Laboratory at INTA, and the NAYADE Gamma Irradiation Facility at CIEMAT. Finally, the authors would like to thank Ministerio de Ciencia e Innovación from the Spanish government for the support of this research via the grant Space Solar Physics RTI2018-096886-B-C52.

## REFERENCES

[1] H. Toyoda, T. Inoue and T. Hara, "Application of liquid crystal on silicon Spatial Light Modulator (LCOS-SLM) for manipulation and sensing," 2015 14th Workshop on Information Optics (WIO), 2015, 1-3, doi: 10.1109/WIO.2015.7206900.

[2] Berghmans F., Decreton M. C., Boueilh D., Reis A. C., Jucker P. and Van Uffelen M., "Space and nuclear environment tolerancing of photonic devices: three European contributions," Proc. SPIE 10288, Advancement of Photonics for Space: A Critical Review (1997)

[3] Solanki, S. K., Iniesta, J. C. del T., Woch, J., Gandorfer, A., Hirzberger, J., Álvarez-Herrero, A., Appourchaux, T., Pillet, V. M., Pérez-Grande, I., Kilders, E. S., Schmidt, W., Cama, J. M. G., Michalik, H., Deutsch, W., Fernandez-Rico, G., Grauf, B., Gizon, L., Heerlein, K., Kolleck, M., et al., "The Polarimetric and Helioseismic Imager on Solar Orbiter," A&A **642**, A11 (2020).

[4] Antonucci, E., Romoli, M., Andretta, V., Fineschi, S., Heinzel, P., Moses, J. D., Naletto, G., Nicolini, G., Spadaro, D., Teriaca, L., Berlicki, A., Capobianco, G., Crescenzio, G., Deppo, V. D., Focardi, M., Frassetto, F., Heerlein, K., Landini, F., Magli, E., et al., "Metis: the Solar Orbiter visible light and ultraviolet coronal imager," A&A **642**, A10 (2020).

[5] Álvarez-Herrero, A., García-Parejo, P., Laguna, H., Villanueva, J., Barandiarán, J., Bastide, L., Reina, M., Sánchez, A., Gonzalo, A., Navarro, R., Vera, I. and Royo, M., "Polarization modulators based on liquid crystal variable retarders for the Solar Orbiter mission," Proc. SPIE 96130I, Polarization Science and Remote Sensing VII (2015).

[6] Capobianco, G., Casti, M., Fineschi, S., Massone, G., Sertsu, M. G., Landini, F., Romoli, M., Antonucci, E., Andretta V., Naletto, G., Nicolini, G., Spadaro, D., Alvarez-Herrero, A., Garcia-Parejo, P., and Marmonti, M "Wide field of view liquid crystals-based modulator for the polarimeter of the Metis/Solar Orbiter," Proc. SPIE 10698, Space Telescopes and Instrumentation 2018: Optical, Infrared, and Millimeter Wave, (6 August 2018)

[7] European Cooperation for Space Standardization (ECSS), "Adoption Notice of ISO 16290, Space systems – Definition of the Technology Readiness Levels (TRLs) and their criteria of assessment," ECSS-E-AS-11C, ESA-ESTEC, Requirements and Standards Division, Noordwijk, The Netherlands, (October 2014)

[8] Álvarez-Herrero, A., Uribe-Patarrollo, N., García-Parejo, P., Vargas, J., Heredero, R. L., Restrepo, R., et al. "Imaging polarimeters based on liquid crystal variable retarder: an emergent technology for space instrumentation," Proc. SPIE, 8160 Polarization Science and Remote Sensing V, (2011).

[9] García-Parejo, P. and Álvarez-Herrero, A., "Liquid crystals for space instrumentation: optical properties of liquid crystal mixtures for polarimeters," Opt. Mater. Express, OME **9**(6), 2681–2698 (2019).

[10] Haellstig, E., Stigwall, J., Lindgren, M. and Sjoqvist, L., "Laser beam steering and tracking using a liquid crystal spatial light modulator," Proc. SPIE, Laser System Technology 5087, (2003).

[11] Wang, X. "Potential of vortex beams with orbital angular momentum modulation for a deep-space optical communication", Opt. Eng. 53(5) 056107 (2014)

[12] Chandra, A. D., Karmakar, M., Nandy, D. and Banerjee, A. "Adaptive hyperspectral imaging using structured illumination in a spatial light modulator-based interferometer," Optics Express 19930, Vol. 30, No. 11, 2022

[13] Silva-López, M., Campos-Jara A. and Álvarez-Herrero A. "Validation of a spatial light modulator for space applications," Proc. SPIE 11180, International Conference on Space Optics, ICSO (2019).

[14] Browar, A. E. M., Shusteff, M., Pana, R. M., Ellis, J. D. and Spadaccini, C. M., "Overview and comparison of spatial light modulator calibration methods," Lawrence Livermore National Laboratory, 31st ASPE annual meeting, 686901. Portland, United States. October 2016.

[15] Silva-López, M., Uribe-Patarrollo, N. and Álvarez-Herrero A. "Advanced iterative algorithm for phase calibration of spatial light modulators integrated in optical instrumentation in a vibration environment." App. Op., Vol. 59, No. 22 (2020)

[16] European Cooperation for Space Standardization (ECSS), "Commercial electrical, electronic and electromechanical (EEE) components," ECSS-Q-ST-60-13C, ESA-ESTEC Requirements and Standards Division, Noordwijk, The Netherlands, (October 2013)

[17] European Cooperation for Space Standardization (ECSS), "Testing," ECSS-E-ST-10C, ESA-ESTEC Requirements and Standards Division, Noordwijk, The Netherlands, (June 2012)

[18] Solar Orbiter – Experiment Interface Document - Part A - SOL-EST-IF-0050 (9 OCT 2007)